Oscillations of algal cell quota: considering two-stage phosphate uptake kinetics

Anglu Shen[a,*], Shufei Gao[b,*], Jie Jiang[b], Qingjing Hu[c], Hao Wang[d], Sanling Yuan[b,**]

[a] *College of Marine Ecology and Environment, Shanghai Ocean University, Shanghai 201306, China*

[b] *College of science, University of Shanghai for Science and Technology, Shanghai 200093, China*

[c] *Yellow Sea Fisheries Research Institute, Chinese Academy of Fishery Sciences, Qingdao 266071, China*

[d] *Department of Mathematical and Statistical Sciences, University of Alberta, Edmonton, Alberta T6G 2G1, Canada*

Abstract

Elucidating the mechanism of the effect of phosphate (P_i) uptake on the growth of algal cells helps understand the frequent outbreaks of algal blooms caused by eutrophication. In this paper, we formulated a comprehensive mathematical model to describe the P_i uptake process of algae incorporating two stages and the transport time delay. The model parameter values are obtained by fitting the long-term experimental data of *Prorocentrum donghaiense* under P_i-sufficient at 20 °C and validated by the experimental data of the proportion of intracellular P_i to the total P_i. Numerical results show that the model reproduces the general characteristics of algal growth and P_i uptake process under P_i-sufficient. According to the experimental and mathematical results, the time delay spent from the surface-adsorbed P_i pool to the intracellular P_i pool is a physiologically plausible mechanism leading to the oscillations of algal cell quota. These results will be helpful for resource managers to predict and deepen their understanding of harmful algal blooms.

Keywords: algal bloom; *Prorocentrum donghaiense*; surface adsorption; transport delay; two-stage model

*Co-first author

**Corresponding author

Email address: sanling@usst.edu.cn (Sanling Yuan)

1. Introduction

Harmful algal blooms (HABs) caused by abnormal proliferation or high biomass accumulation or other toxic microalgae at the sea surface or in the water column have brought deleterious impacts on aquaculture, fisheries, tourism, human health, and components of aquatic ecosystems (Anderson, 1997; Anderson et al., 2012; Hallegraeff, 1993). About 300 species of phytoplankton are the bloom-forming species, while only 40 or so species have the capacity to produce potent toxins, and most of them are dinoflagellates (Hallegraeff, 1993). The coastal water in the East China Sea (ECS) and Yangtze River Estuary (YRE) is one of the famous regions with frequent HABs events since the 1980s (Chen & Chen, 2021; Yu et al., 2017). The dinoflagellate *Prorocentrum donghaiense* (formerly named *P. shikokuense*; (Gómez et al., 2021; Lu & Goebel, 2001; Lu et al., 2022)) is a major dinoflagellate species that have formed blooms in the coastal waters of the ECS each year since 2000 during late April-May (Lu et al., 2022; Tang et al., 2006; Yu et al., 2017; Zhou et al., 2017c). The scale (approximately 10000 km^2) and length of time (approximately one month) of the *P. donghaiense* blooms have been amazing for some years (Yu et al., 2017; Zhao, 2010). Like other HABs, *P. donghaiense* blooms may be great harmful to the ecosystem and fishery resources. This is often due to the accumulation of algal biomass, which produces toxic scum and foam, covering other phytoplankton and sea grass beds, and causing animal death through decay and oxygen consumption (Anderson et al., 2012). Laboratory and field studies have shown that the *P. donghaiense* blooms are extremely harmful to the survival of zooplankton and scallop (Chen et al., 2007; Lin et al., 2015; Shen et al., 2022). Furthermore, during the *P. donghaiense* blooms, the community structure of zooplankton changes significantly, from being copepod and jellyfish-dominated to small jellyfish-dominated (Lin et al., 2014), and it is well known that copepods are

the main food source for many fish larvae (Uye et al., 1999). Therefore, elucidating the growth characteristics of *P.donghaiense* will help better to understand its possible effects on the ECS and YRE ecosystems.

Due to widespread nutrient loading such as phosphate (P_i), the eutrophication of aquatic ecosystems throughout the world leads to the appearance of HABs (Anderson et al., 2002; Xiao et al., 2019; Zhou et al., 2017b). In the ECS and YRE, diatom blooms and dinoflagellate blooms often appear alternatively (diatom-dinoflagellate-diatom) from April to August, where P_i plays an important role in this succession. Diatom blooms (such as *Skeletonema costatum*) occur in early spring when P_i is sufficient because diatom has a greater advantage in P_i affinity, and the growth demand for P_i is also higher. Therefore, the growth of diatom algal blooms quickly collapses after P_i depletion (Ou et al., 2008; Zhou et al., 2017c). Dinoflagellates blooms such as *P. donghaiense* blooms have been observed in the coastal waters of the ECS from late April to June after diatom blooms when the P_i is insufficient because *P. donghaiense* has lower thresholds of P_i and could make good use of the metabolized dissolved organic phosphate or phagocytose the organic debris (Ou et al., 2008; Yu et al., 2017). This can be verified in the research by Lu & Li (2006), where the authors obtained that the luxury coefficient of P_i ($R_P = Q_{\max}/Q_{\min}$, 4.3) of *P. donghaiense* was higher than that of *S. costatum* (2.5), and its growth potential of storage P_i ($t_P = \ln R_P/\mu_{\max}$, 2.08 day) was higher than that of *S. costatum* (0.53 day). This also indicates that P_i is a nutrient limiting phytoplankton biomass, which plays an important role in the long-lasting spring bloom of *P. donghaiense* in the ECS and YRE (Shen et al., 2019; Yu et al., 2017). Thus, by studying the uptake of P_i by algae, we can find an effective way to control algal bloom formation and biomass accumulation (Kilham & Hecky, 1988; Parslow et al., 1985; Schindler et al., 2008).

The previous studies on P_i uptake by algae commonly focus on various culture environments such as external P_i concentration, illumination intensity, flowing rate, and temperature (Robarts & Zohary, 1987; Shen et al., 2016; Shi et al., 2015), and partition the growth of algae, especially in bloom, into four phases: slowly-growing, exponentially-growing, stable, and dissipation phases (Tester & Steidinger, 1997). In a field survey covering the process of a *P. donghaiense* bloom in the coastal waters of ECS from 9 to 20 May 2016, we observed the oscillation phenomenon in the cell density of *P. donghaiense* (Shen et al., 2019). It seems crucial to understand the mechanism leading to oscillations in the algal growth process since it could provide a new perspective to the research on the specific P_i demands and abilities to assimilate P_i by algae which helps predict algal blooms more accurately (Droop, 1983). However, as far as we know, few studies paid attention to the oscillations of cell density and cell quota appearing during the algae culture (Caperon, 1969; Cunningham & Maas, 1978; Droop, 1983; Muhammadu et al., 2017).

Additionally, recent researches have shown that there are two P_i pools, surface-adsorbed P_i (AP) pool and the intracellular P_i (QP) pool in the microalgae (Jiang et al., 2019; Jin et al., 2021; Sañudo-Wilhelmy et al., 2004; Xing et al., 2021; Yao et al., 2011; Zhou et al., 2017a). Sañudo-Wilhelmy et al. (2004) suggested that AP may be part of a two-step process in which surface adsorption is followed by internalization in the QP pool. Partitioning the total P_i into AP and QP is essential to study P_i uptake kinetics of algae. This is contrasted with the studies only that consider transport from the substrate into cells (Saxton et al., 2012). Jin et al. (2021) showed that the cell-associated P_i content of phytoplankton washed with oxalic acid was significantly lower than that of unwashed phytoplankton. This result indicated that the cell surface P_i pool removed by oxalic acid reagent has a non-negligible proportion in the total P_i pool of phytoplankton cells. In addition, new evidences

demonstrate that phytoplankton Redfield ratios are strongly affected by partitioning total P_i into surface-adsorbed and intracellular P_i pools (Button, 1978; Fu et al., 2006; Sañudo-Wilhelmy et al., 2004). Thus, the considerations of both surface-adsorbed and intracellular P_i pools may be required since Redfield ratios in the ocean reflect the chemical composition of N-fixing organisms (Kay & Mahlburg-Kay, 1991). Finally, in the modeling process of P_i uptake kinetics, distinguishing the surface-adsorbed P_i pool and intracellular P_i pool can more accurately reflect the characteristics of P_i uptake by phytoplankton (Gao et al., 2022; Jiang et al., 2019; Yao et al., 2011).

In this paper, we first develop a novel two-stage P_i uptake model incorporating the time delay spent from the surface-adsorbed P_i pool to the intracellular P_i pool. Then the model is calibrated and validated by the long-term experimental data of *P. donghaiense* under P_i-sufficient at 20 °C. Furthermore, combining with the experimental and mathematical results, one plausible physiology mechanism leading to algal cell quota oscillations is proposed. Finally, the ratio of intracellular P_i to total P_i is also discussed since the study of stoichiometry flexibility on total P_i partitioning helps understand the specific P_i uptake process of algae.

2. Materials and methods

2.1. Model description

Phosphate uptake by algae may be seen as a two-stage process. Firstly, P_i in the substrate is adsorbed on algal cell surfaces and stored in the AP pool. Secondly, surfaced-adsorbed P_i enters the QP pool through the active transport of membrane and then is assimilated to form newborn algal cells. In this paper, A (10^8 cells L^{-1}) represents the algal cell density and N (μmol L^{-1}) represents the P_i concentration in the substrate. S (10^{-8}μmol $cell^{-1}$) and Q (10^{-8}μmol $cell^{-1}$) represent the

cell quota of AP and QP, respectively.

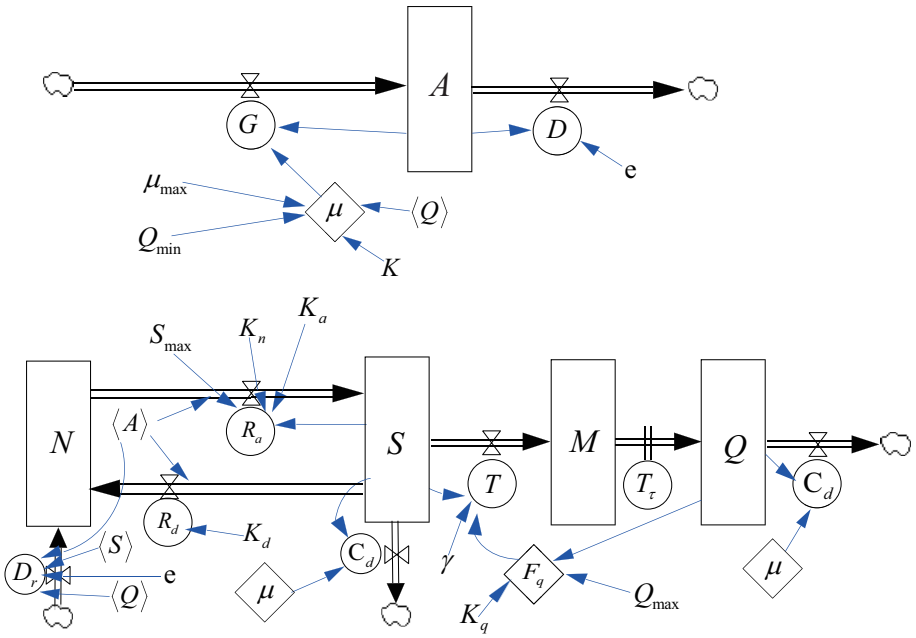

Figure 1: Two-stage model concept map. Boxes represent levels; circles represent rates; diamonds and square brackets are auxiliaries and shadow variables, respectively. There is a delay τ in the transport process from AP to QP. The biological meanings and functions of these notations in Fig. 1 are shown below the brace in model (1).

In the early P_i uptake model proposed by Droop (1973), it is assumed that the algal specific growth rate (μ) is a function of the cell quota of intracellular P_i:

$$\mu = \mu_{\max}\left(1 - \frac{Q_{\min}}{Q}\right),$$

where $\mu_{\max}$ is the maximum growth rate of algae, $Q_{\min}$ is the minimum cell quota of intracellular P_i. Empirical evidence shows that the Droop form describes data more accurately than the Monod form (Wang et al., 2022). Under fixed light intensity, the self-shading among algal cells will limit its growth rate with the increase of algal cell density. Therefore, the algal specific growth rate can be rewritten as:

$$\mu = \mu_{\max}\left(1 - \frac{Q_{\min}}{Q}\right)(1 - \frac{A}{K}),$$

where K is the constant carrying capacity that depends on external factors bounding algae density (e.g. light and nutrients). The loss rate of algal cells due to natural mortality is assumed to be proportional to its density and determined by the death rate e. So the change rate of A can be expressed as:

$$\frac{\mathrm{d}A}{dt} = \mu A - eA.$$

We assume that the P_i adsorption by algal cells is a single-layer process, and surface-adsorbed P_i can be desorbed into the substrate with a rate of K_d. The P_i adsorption rate of algal cells is limited by the surface area of algal cells and the density of sorption sites, i.e., there is a saturated concentration of P_i on the cell surface. In addition, the adsorption rate of P_i by algae was also affected by the P_i concentration in the substrate. Here, to simplify the model, we assume that the surface properties of algal cells (e.g. cell size and density of sorption sites) are uniform and ignore cell-specific differences. Based on these assumptions, the P_i adsorption process can be described by the following function,

$$R_a = K_a S \left(1 - \frac{S}{S_{\max}}\right) \frac{N}{N + K_n},$$

where K_a is the adsorption rate, $S_{\max}$ is the maximum cell quota of surface-adsorbed P_i, K_n is the half-saturation coefficient of algal nutrient adsorption. Since the surface-adsorbed P_i pool and intracellular P_i pool are considered two separated compartments, so the transport rate from the AP pool to the QP pool can be described as one-order rate compartment model (Cembella et al., 1984; Droop, 1983):

$$T = \gamma S,$$

where γ is the maximum specific nutrient uptake rate of algae. Furthermore, the transport process of P_i is also controlled by the feedback of the size of the intracellular P_i pool, which can be described

by the below sigmoid feedback function (Flynn, 2003; John & Flynn, 2000; Yao et al., 2011):

$$F(Q) = \frac{\left(1 - \frac{Q}{Q_{\max}}\right)^4}{\left(1 - \frac{Q}{Q_{\max}}\right)^4 + K_q},$$

where $Q_{\max}$ and K_q are the maximum cell quota of intracellular P_i and the constant in the feedback function, respectively. Thus, the transport rate T can be written as:

$$T = \gamma \frac{\left(1 - \frac{Q}{Q_{\max}}\right)^4}{\left(1 - \frac{Q}{Q_{\max}}\right)^4 + K_q} S.$$

With the division of algal cells, the cell quota of surface-adsorbed P_i will be diluted accordingly, and the dilution rate is proportional to the specific growth rate μ (Wang et al., 2007). Thus the change rate of S at time t can be described as:

$$\frac{\mathrm{d}S}{\mathrm{d}t} = R_a - T - \mu S.$$

In addition, the time delay τ from AP pool transport into the QP pool should be considered when researching the P_i uptake process of algal cells (Fu et al., 2006). Hence, at time t, the final form of P_i uptake rate per algal cell is

$$T_\tau = \gamma \frac{\left(1 - \frac{Q_\tau}{Q_{\max}}\right)^4}{\left(1 - \frac{Q_\tau}{Q_{\max}}\right)^4 + K_q} S_\tau,$$

where the notation Q_τ means $Q(t - \tau)$.

In order to make our model closed, a new process variable M (10^{-8}μmol cell^{-1}) is introduced to represent the cell quota of P_i in the transport process. Due to the existence of the transport delay of P_i from the cell surface into the cell, the change rate of M at time t can be expressed as:

$$\frac{\mathrm{d}M}{\mathrm{d}t} = T - T_\tau.$$

Table 1: Parameters in model (1).

Parameter	Units	Explanation
$\mu_{\max}$	day^{-1}	Maximum specific growth rate of algae
$Q_{\min}$	μmol cell^{-1}	Minimum cell quota of intracellular P_i
K	cells L^{-1}	Resource carrying capacity determined by nutrient and light
e	day^{-1}	Death rate of algae
γ	day^{-1}	Maximum specific nutrient uptake rate of algae
τ	day	Time needed for P_i in surface-adsorbed P_i pool coming into intracellular P_i pool
$Q_{\max}$	μmol cell^{-1}	Maximum cell quota of intracellular P_i
K_q		Constant in the feedback function
K_a	day^{-1}	Adsorption rate
K_d	day^{-1}	Desorption rate
$S_{\max}$	μmol cell^{-1}	Maximum cell quota of surface-adsorbed P_i
K_n	μmol L^{-1}	Half-saturation coefficient of algal nutrient adsorption
r		Decomposition ratio of dead algal cells

Since the algal cell quota dilution rate is proportional to the algal growth rate (Wang et al., 2007), so the change rate of Q with time is governed by P_i uptake rate of algae (T_τ) and the cell-specific growth rate (μ) (Droop, 1973). Hence, the change rate of Q at time t can be described as:

$$\frac{dQ}{dt} = T_\tau - \mu Q.$$

For the dead algal cells, we assume that part of them can be decomposed and the intracellular P_i and surface-adsorbed P_i can be released into the substrate for recycling (Tiwari et al., 2017; Wang et al., 2008). Therefore, the change rate of N at time t can be expressed as:

$$\frac{dN}{dt} = reA(Q+S) - R_a A + K_d A,$$

where r is the decomposition ratio of dead algal cells.

Based on the above assumptions, we have the following novel P_i uptake kinetics model,

$$\begin{cases} \dfrac{\mathrm{d}A}{\mathrm{d}t} = \underbrace{\underbrace{\mu_{\max}\left(1-\dfrac{Q_{\min}}{Q}\right)\left(1-\dfrac{A}{K}\right)}_{\mu\text{: specific growth rate}}A}_{G\text{: cell growth}} - \underbrace{eA}_{D\text{: cell death}}, \\ \dfrac{\mathrm{d}Q}{\mathrm{d}t} = \underbrace{\gamma\dfrac{\left(1-\frac{Q_\tau}{Q_{\max}}\right)^4}{\left(1-\frac{Q_\tau}{Q_{\max}}\right)^4+K_q}}_{F_q\text{: feedback function}}S_\tau - \underbrace{\mu_{\max}\left(1-\dfrac{Q_{\min}}{Q}\right)\left(1-\dfrac{A}{K}\right)Q}_{C_d\text{: cell quota dilution due to cell division}}, \\ \dfrac{\mathrm{d}M}{\mathrm{d}t} = \gamma\dfrac{\left(1-\frac{Q}{Q_{\max}}\right)^4}{\left(1-\frac{Q}{Q_{\max}}\right)^4+K_q}S - \gamma\dfrac{\left(1-\frac{Q_\tau}{Q_{\max}}\right)^4}{\left(1-\frac{Q_\tau}{Q_{\max}}\right)^4+K_q}S_\tau, \\ \dfrac{\mathrm{d}S}{\mathrm{d}t} = \underbrace{K_a S\left(1-\dfrac{S}{S_{\max}}\right)\dfrac{N}{N+K_n}}_{R_a\text{: absorption from substrate}} - \underbrace{K_d S}_{R_d\text{: desorption}} - \underbrace{\gamma\dfrac{\left(1-\frac{Q}{Q_{\max}}\right)^4}{\left(1-\frac{Q}{Q_{\max}}\right)^4+K_q}S}_{T\text{: } P_i \text{ transport rate}} - \underbrace{\mu_{\max}\left(1-\dfrac{Q_{\min}}{Q}\right)\left(1-\dfrac{A}{K}\right)S}_{C_d\text{: cell quota dilution due to cell division}}, \\ \dfrac{\mathrm{d}N}{\mathrm{d}t} = \underbrace{reA(Q+S)}_{D_r\text{: } P_i \text{ recycling from dead algal cells}} - K_a S\left(1-\dfrac{S}{S_{\max}}\right)\dfrac{N}{N+K_n}A + K_d S A. \end{cases} \tag{1}$$

where the biological meanings and units of parameters are listed in Table 1. The conceptual diagram of model (1) is shown as Fig. 1. For the model's integrity, we introduce the process variable M.

However, it dose not affect on the kinetics of P_i uptake. Therefore, the model can be simplified as:

$$\begin{cases} \dfrac{\mathrm{d}A}{\mathrm{d}t} = \underbrace{\underbrace{\mu_{\max}\left(1-\dfrac{Q_{\min}}{Q}\right)\left(1-\dfrac{A}{K}\right)}_{\mu\text{: specific growth rate}}A}_{G\text{: cell growth}} - \underbrace{eA}_{D\text{: cell death}}, \\ \dfrac{\mathrm{d}Q}{\mathrm{d}t} = \underbrace{\gamma\dfrac{\left(1-\frac{Q_\tau}{Q_{\max}}\right)^4}{\left(1-\frac{Q_\tau}{Q_{\max}}\right)^4+K_q}}_{F_q\text{: feedback function}}S_\tau - \underbrace{\mu_{\max}\left(1-\dfrac{Q_{\min}}{Q}\right)\left(1-\dfrac{A}{K}\right)Q}_{C_d\text{: cell quota dilution due to cell division}}, \\ \dfrac{\mathrm{d}S}{\mathrm{d}t} = \underbrace{K_aS\left(1-\dfrac{S}{S_{\max}}\right)\dfrac{N}{N+K_n}}_{R_a\text{: absorption from substrate}} - \underbrace{K_dS}_{R_d\text{: desorption}} - \underbrace{\gamma\dfrac{\left(1-\frac{Q}{Q_{\max}}\right)^4}{\left(1-\frac{Q}{Q_{\max}}\right)^4+K_q}}_{T\text{: } P_i \text{ transport rate}}S - \underbrace{\mu_{\max}\left(1-\dfrac{Q_{\min}}{Q}\right)\left(1-\dfrac{A}{K}\right)S}_{C_d\text{: cell quota dilution due to cell division}}, \\ \dfrac{\mathrm{d}N}{\mathrm{d}t} = \underbrace{reA(Q+S)}_{D_r\text{: } P_i \text{ recycling from dead algal cells}} - K_aS\left(1-\dfrac{S}{S_{\max}}\right)\dfrac{N}{N+K_n}A + K_dSA. \end{cases} \tag{2}$$

2.2. Materials and methods

2.2.1. Algal culture conditions

Prorocentrum donghaiense was provided by Douding Lu of the Second Institute of Oceanography, Ministry of Natural Resources of the People's Republic of China (MNR) in Hangzhou, China. These algal cells were pre-cultured at 20 °C in f/2 medium (Guillard, 1975). The light intensity and light : dark cycle of these cultures were 65-70 μmol photons m^{-2} s^{-1} and 12 : 12 h, respectively. All cultures were performed in an illumination incubator. The cultures were shaken vigorously twice times daily within the set time in case the algal cells gathered at the bottom. The algal cells used in the following experiments were those cultured to exponential growth phase.

2.2.2. Phosphate uptake experiments

The initial cell density of these batch cultures was about 0.15×10^8 cells L^{-1}, and the initial P_i concentration is 35.08 μM. Three biological repeats were used in the P_i uptake experiments.

A 10 mL sample was collected every 3 days (0, 3, 6, 9, 12, 15, 18, 21, 24, 27, and 30 day). The determination methods of N, AP, and QP were based on Yao et al. (2011) and Jiang et al. (2019) with slightly modifications. The cell density (A) was counted in accordance with Jiang et al. (2019).

2.3. Statistical analysis

The experimental data are presented as the mean ± SE of triplicates, which follows the normal distribution with homogeneous variance (Levene tests). One-way ANOVA and Tukeys multiple range test were used to analyze the statistical differences between sample days. p values < 0.05 were considered statistically significant. All analyses were performed using IBM SPSS Statistics 22.0 (IBM SPSS Software, Chicago, USA), and all pictures are drawn by MATLAB (R2016b).

2.4. Model calibration and validation

Based on the long-term experimental data of *P. donghaiense*, The parameter values of model (2) are estimated by the least square method. This process is implemented by the "fmincon" function of MATLAB (R2016b). The following objective function is used in this study,

$$f(\Phi, m) = \frac{1}{m}\sum_{i=1}^{m} cost_i,$$

where Φ is a vector of parameters to be calibrated, m is the number of model variables used for model calibration at the same time. $cost_i$ is the model cost of the ith state variable (Adhurya et al., 2021; Gao et al., 2022),

$$cost_i = \sum_{j=1}^{n} \frac{(X_{ij}^{sim} - X_{ij}^{obs})^2}{X_{ij}^{obs^2}},$$

where n is the number of observed values of a variable, X_{ij}^{sim} and X_{ij}^{obs} are respectively the simulation value and the observed value of the ith state variable at day j. After model calibration, experimental

data of QP/(QP + AP) (the ratio of intracellular P_i to total P_i) was used for model validation. Moreover, the relative errors of all model variables were also calculated to measure the model's fitness. The relative error of the ith state variable of model is calculated by the below equation (Marois & Mitsch, 2016):

$$RE_i = \frac{1}{n}\sum_{j=1}^{n}\left(\frac{X_{ij}^{sim}}{X_{ij}^{obs}} - 1\right) \times 100.$$

3. Results

3.1. Experimental data and fitting results

The model fitting results and experimental data of the four state variables of A, N, Q and S of *P. donghaiense* at 20 °C under P_i-sufficient condition are shown in Fig. 2. The estimate parameter values are listed in Table 2. Table 3 shows the model costs and relative errors for each state variable of model (2) during the calibration and validation. It can be seen from Fig. 2, with the initial 0.15×10^8 cells L^{-1}, A declined in the first 3 days, increased slowly in the next 6 days and then increased significantly ($p < 0.05$) from day 9 to day 15 and reached a peak value on day 15, finally reached another peak value on day 27. With the initial P_i concentration in substrate 35.08 μM, N decreased throughout the experiment, rapidly in the first 20 days and slowly in the last 10 days. With the initial 9.43×10^{-8} μmol $cell^{-1}$, Q shows a significant trend of fluctuation ($p < 0.05$), and the fluctuation range is gradually decreasing. With the initial 13.53×10^{-8} μmol $cell^{-1}$, S shows a downward fluctuation trend during the experiment, and the fluctuation range is also gradually decreasing. In detail, S increased significantly ($p < 0.05$) in the first 3 days, obtained a maximum value of 24.57×10^{-8} μmol $cell^{-1}$ on day 3, decreased fast in the next 9 days, and then emerged the phenomenon of oscillation in the last 18 days.

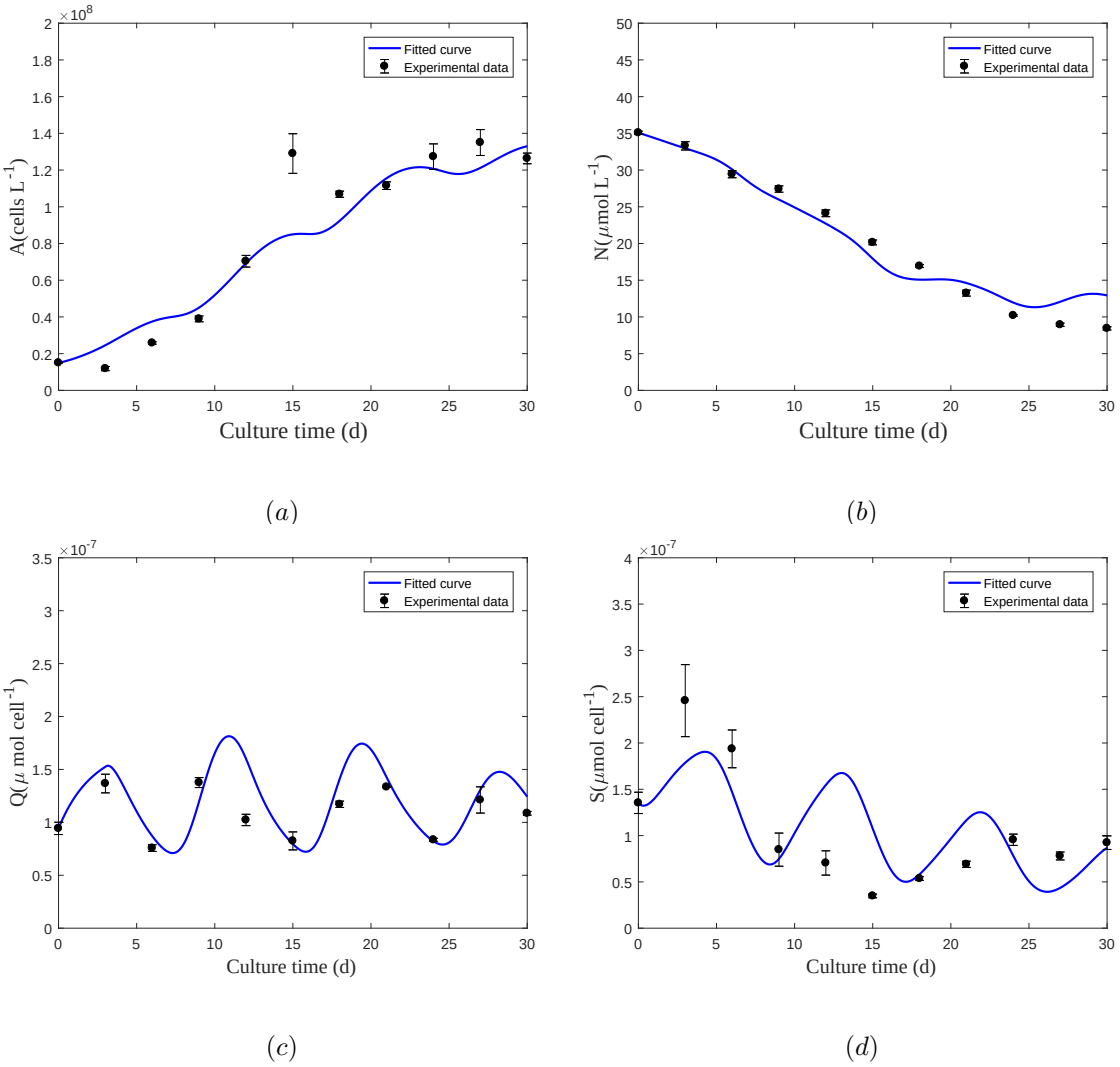

Figure 2: Comparison of model fitted curve and experimental data of *P. donghaiense* at 20 °C under P_i sufficient condition. (a) cell density (A); (b) P_i in the substrate (N); (c) the cell quota of QP (Q); (d) the cell quota of AP (S). The parameters of model (2) can be estimated by fitting the four state variables simultaneously, and the values are shown in Table 2. The experimental data is expressed as mean ± SE.

Table 2: Parameter values of model (2) estimated from experimental data of A, Q, S and N in *P. donghaiense*.

Parameter	Unit	Value
$\mu_{\max}$	day^{-1}	0.52
$Q_{\min}$	$\mu\text{mol cell}^{-1}$	3.8×10^{-8}
K	cells L^{-1}	2.8×10^{8}
e	day^{-1}	0.175
γ	day^{-1}	2.23
$Q_{\max}$	$\mu\text{mol cell}^{-1}$	18.8×10^{-8}
τ	day	3.05
K_q		0.23
K_a	day^{-1}	1.92
K_d	day^{-1}	0.28
K_n	$\mu\text{mol L}^{-1}$	14.3
$S_{\max}$	$\mu\text{mol cell}^{-1}$	39.5×10^{-8}
r		0.92

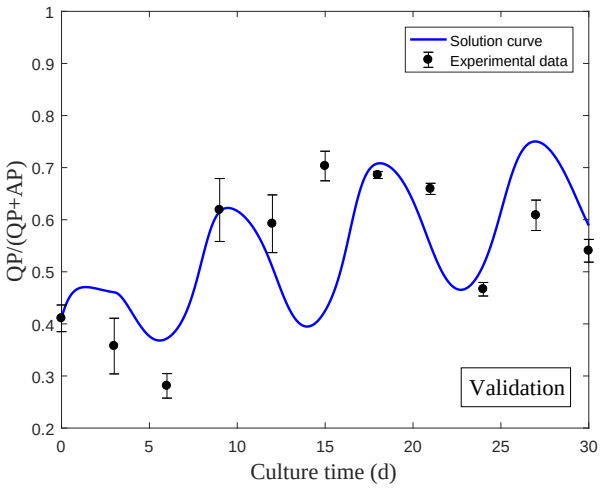

Figure 3: Validation of model (2) with the data of the ratio of intracellular P_i to total P_i (QP/(QP+AP)). Here the parameter values from Table 2. The experimental data is expressed as mean ± SE.

Combining model cost and relative error, it can be seen from Fig. 2, Q has the best simulation effect among the four variables, with the smallest model cost 0.45. The cell density of algae (A) and the substrate P_i concentration (N) also fit well and the relative errors are 1.53 and 0.48, respectively. For S, the simulated curve is basically consistent with the experimental data, especially the first peak (day 3) and the last 12 days. But, on the day 12 to day 15, the fitting curve of model (2) is much higher than the experimental data.

Table 3: Model costs and relative errors of all variables.

State variable	Model cost	Relative error
A	1.54	10.24
Q	0.45	10.43
S	6.64	24.95
N	0.48	7.61
$\frac{\mathrm{QP}}{\mathrm{QP+AP}}$	0.45	1.97

Furthermore, we use the experimental data of QP/(QP+AP) to validate model (2), where the model parameter values are from Table 2 and the initial values of A, N, Q, S, are 0.15×10^{8}, 35.08, 9.43×10^{-8}, and 13.53×10^{-8}, respectively. Fig. 3 shows that the solution of model (2) is well in agreement with the experimental data and can simulate the trend of the experimental data. The model cost and relative error are 0.45 and 1.97, respectively. The calibration and validation results showed that the two-stage P_i uptake model with transport delay could well describe the P_i uptake characteristics of *P. donghaiense* at 20 °C under P_i-sufficient condition.

3.2. Sensitivity analysis

To provide a comprehensive understanding the influence of different input parameter values and their variations on the model results, the sensitivity analysis of model (2) solutions for all variables, with respect to some important model parameters, namely, the maximum specific growth rate of algal cells ($\mu_{\max}$), the minimum cell quota of intracellular P_i ($Q_{\min}$), the adsorption rate of P_i on cell surface (K_a), and the decomposition ratio of dead algal cells (r), respectively. The parameter's baseline values are from Table 2. For this purpose, we derive the sensitivity system of the partial derivative of the variable $X = \{A, N, Q, S\}$ of model (2) with respect to the parameters $q = \{\mu_{\max}, Q_{\min}, K_a, r\}$ (the detail methods please see Ref. (Bortz & Nelson, 2004)).

The semi-relative sensitivity solutions ($q\frac{\partial X}{\partial q}$) for all state variables of model (2) are displayed in Fig. 4. It is worth noting that the information presented in Fig. 4 is not equivalent to the difference between the solution in Fig. 2 and the solution in model (2) with a slight increase in the parameters, but rather depicts a time series diagram of the derivatives of the state variables with respect to the selected parameters. From the semi-relative sensitivity solutions, we can observe that r has a positive effect on all variables of model (2), with the greatest effect on the P_i concentration

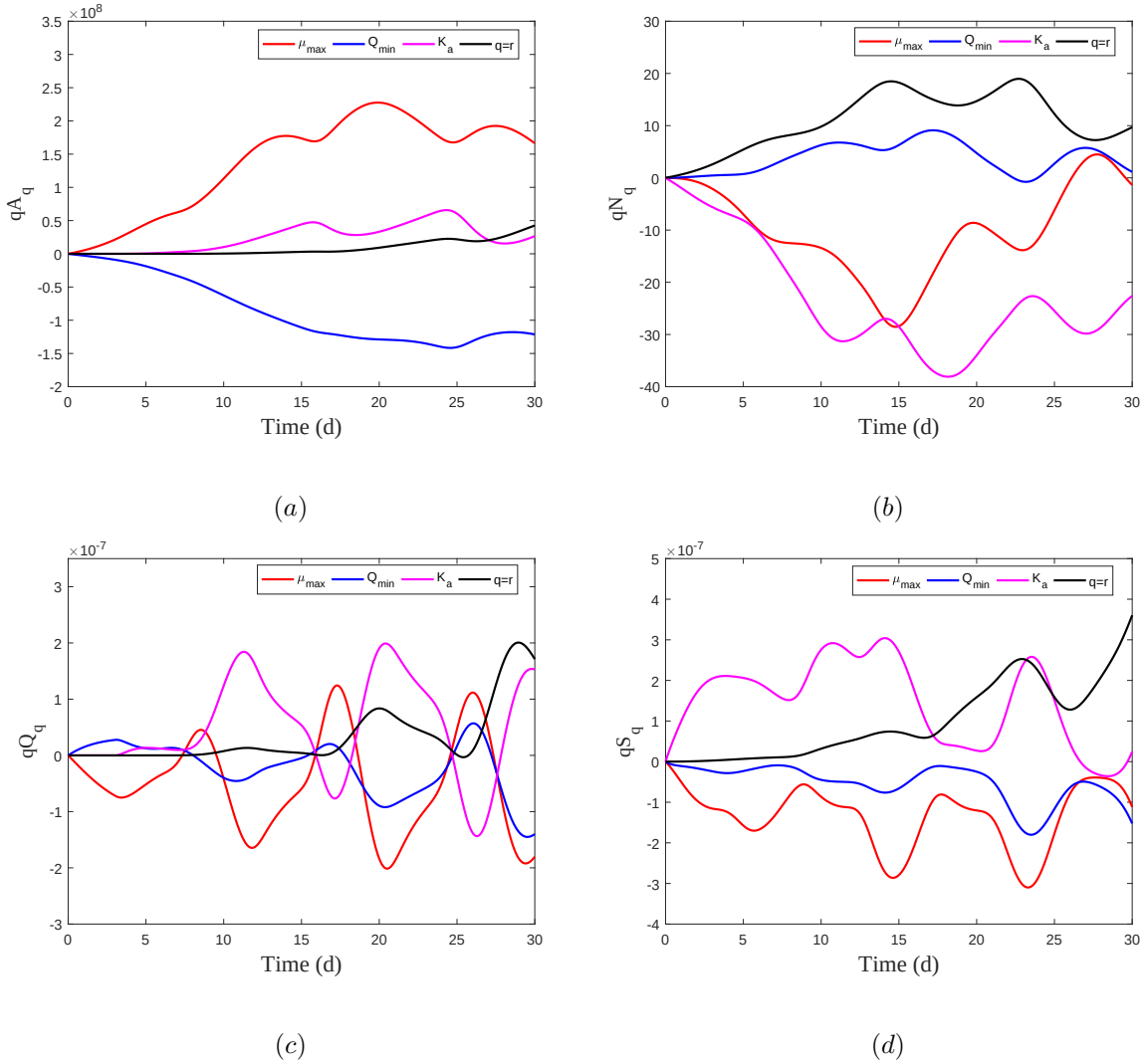

Figure 4: The semi-relative sensitivity solutions ($q\frac{\partial X}{\partial q}$) for four variables of model (2), with respect to the important model parameters, namely, the maximum specific growth rate of algal cells ($\mu_{\max}$), the minimum cell quota of intracellular P_i ($Q_{\min}$), the adsorption rate of P_i on cell surface (K_a), and the decomposition ratio of dead algal cells (r), respectively. The parameter values are shown in Table 2.

in the substrate. For the other three variables, the effect of r is very small in the early stage but with an increasing effect over time. This may be because P_i in the substrate is heavily consumed by the early stage of the experiment, thus the decomposition of dead cells becomes an important P_i source for cell growth in the last stage of the experiment. Furthermore, we can observe that $\mu_{\max}$ and K_a have positive effects on algal cell density, while $Q_{\min}$ plays a negative role. In the initial stage, the three parameters had little effect on cell density, gradually increased over time, and finally decreased. The effect of $\mu_{\max}$ on cell density reached the maximum value at day 20 (Fig. 4a), and a doubling of $\mu_{\max}$ will yield an increase of cell density of about 2.28×10^8 at this time. The effect of $\mu_{\max}$ gradually decreased after day 20, which may be due to the growth rate of algae is mainly limited by light and resources at the last stage of the experiment. $Q_{\min}$ is minimal internal P_i concentration to maintain cell growth, so its increase will lead to a decrease in cell density and a positive effect on P_i concentration in the substrate. The influence of K_a and $\mu_{\max}$ on P_i concentration in substrate is negative, and the effect increased first and then decreased with time. The influence of the parameters $\mu_{\max}$, $Q_{\min}$ and K_a on Q is very complex. It can be positive or negative over time, and the amplitude increases gradually. For S, $Q_{\min}$ and $\mu_{\max}$ play negative roles, while K_a has a positive effect in the initial stage and finally becomes negative, which may be caused by the time delay of P_i transport from the cell surface to the intracellular.

The logarithmic sensitivity curves ($\frac{\partial X}{\partial q}\frac{q}{X}$) for all state variables of model (2) are displayed in Fig. 5. From the log-sensitivity solution curve, we can explain the percentage of solution change caused by positive perturbation of the parameter. As can be seen from Figs. 4 and 5, the semi-relative sensitivity solution and the logarithmic sensitivity solution have similar trends, but they represent different meanings. For algal density, $\mu_{\max}$ still has the most positive effect, and changes in $\mu_{\max}$

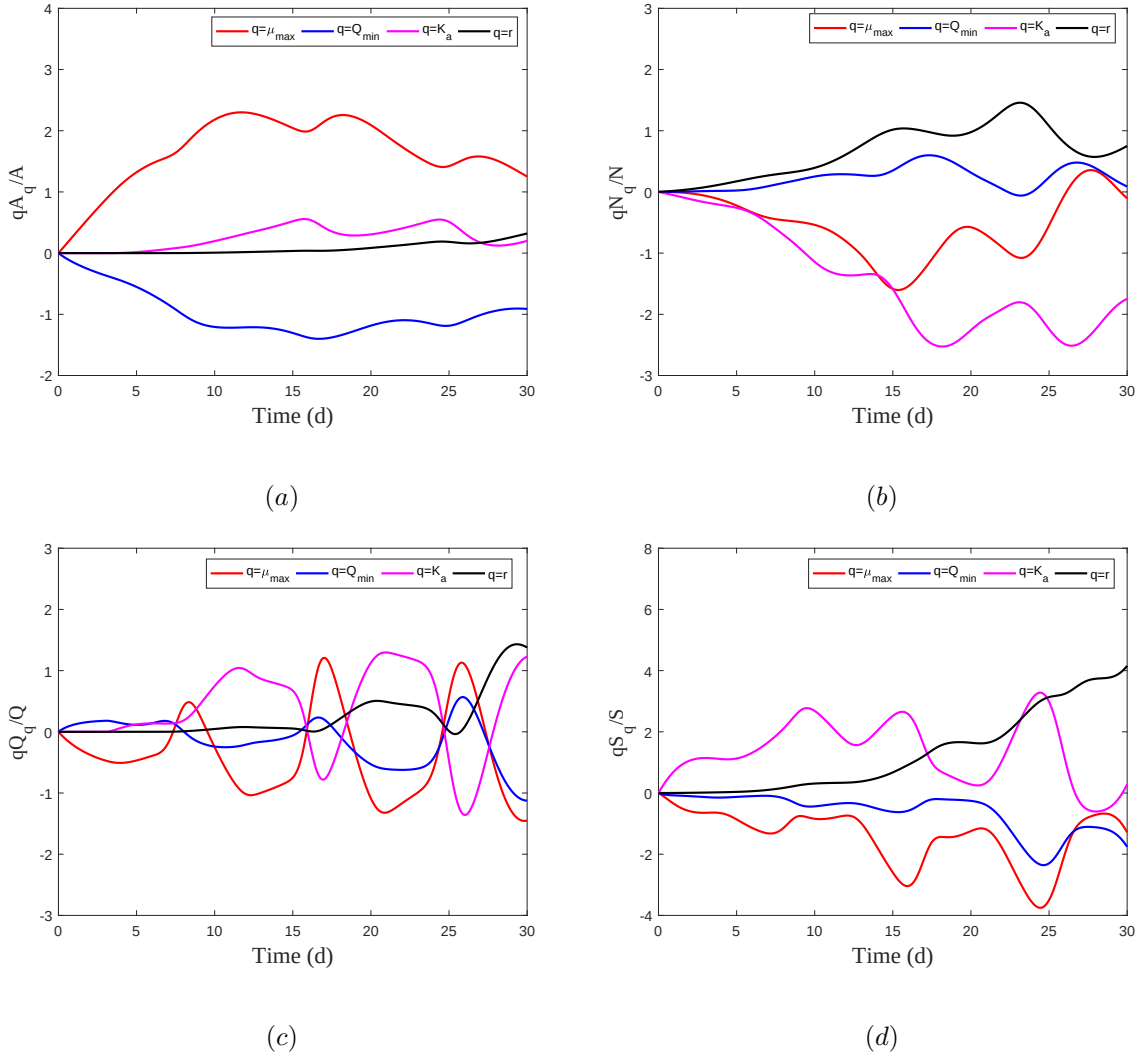

Figure 5: The logarithmic sensitivity solutions ($\frac{\partial X}{\partial q}\frac{q}{X}$) for four variables of model (2), with respect to the important model parameters, namely, the maximum specific growth rate of algal cells ($\mu_{\max}$), the minimum cell quota of intracellular P_i ($Q_{\min}$), the adsorption rate of P_i on cell surface (K_a), and the decomposition ratio of dead algal cells (r), respectively. The parameter values are shown in Table 2.

can cause changes in A above 200% at day 11. K_a has the most significant adverse effect on N, and a change of K_a will cause changes in N about 252% at day 18. In addition, Fig. 5d suggested that the parameter r causes more than 400% change in the solution of S at day 30.

4. Discussion

In this paper, we developed a novel model based on the two-stage model of (Jiang et al., 2019) by further incorporating the transport delay from surface-adsorbed P_i pool to intracellular P_i pool and the decomposition process of dead algal cells. The model was calibrated and validated by the long-term experimental data of *P. donghaiense* under P_i-sufficient condition at 20 °C. The validity of model (2) has been confirmed for the intuitive fitting results, model costs, and relative errors. The sensitivity analysis of the model was carried out with the parameter values in Table 2. These results show that the maximum specific growth rate $\mu_{\max}$ is the most sensitive parameter for the density of algal cells, and the adsorption rate K_a has the most negative effect on P_i concentration in the substrate. We proposed a possible physiological mechanism from mathematical and experimental results that may lead to oscillations of algal cell quota. The transport delay τ between surface-adsorbed P_i pool to intracellular P_i pool may cause the fluctuations of Q and S. These results match those observed in earlier studies (Caperon, 1969; Cunningham & Maas, 1978; Misra et al., 2020). Cunningham & Maas (1978) showed that the complex delay between the two different physiological components between the cell division rate and the environmental limiting nutrient concentration would cause the oscillation growth of algae cells. Any delay arising from accumulated time constants may cause instability, for oscillation may be expected in any control system when there is a phase change between receipt of information and response to it (Droop, 1983). Some studies have shown

that many algal cells have the "luxury uptake" of P_i and store it in the form of PolyP (Solovchenko et al., 2019; Sun et al., 2014). The key to developing the "luxury uptake" process would be via co-regulation of P_i signal transduction pathways between intracellular P_i pool and surface-adsorbed P_i and hydrolysis of PolyP to P_i, which needs a time lag for the specific biochemical process (Kornberg et al., 1999).

In addition, following the modeling ideas of Jiang et al. (2019) and Yao et al. (2011), the cell surface P_i pool and intracellular P_i pool are considered two independent compartments in our model. Studies have shown that the cell surface P_i pool has a significant proportion of the total P_i pool of algal cell. Our experimental results show that the proportion range of surface P_i pool to the total P_i pool of *P.donghaiense* is $3-72\%$ under P_i sufficient condition, in the range of previously reported values. Qu et al. (2020) reported that the ratio of cell surface phosphorus pool to total phosphorus pool of *P. donghaiense* could reach $9-72\%$ in P_i sufficient laboratory culture. The proportion of P_i pool on the cell surface of wild phytoplankton samples ranged from 7% to 36% in the Sanggou Bay (Xu & Liu, 2016), 15% to 46% in the Delaware Inland Bays and Delaware River Estuary (Fu et al., 2005), 0.7% to 34% in Lake Erie (Saxton et al., 2012), and 4% to 54% in the Yellow sea (Jin et al., 2021). Sañudo-Wilhelmy et al. (2004) indicated that the proportion of surface-adsorbed P_i in the senescent phase of *Thalassiosira weissflogii* can reach 90%, significantly higher than that in the exponential growth phase (30%). As shown in Fig. 3, model fitting results show that the solution of model (2) can be well agreement with the experimental data of QP/(QP+AP), where the parameter values are from Table 2. In addition, the proportion of intracellular P_i to total P_i showed a fluctuating trend during algae culture (Fig. 3). The distribution of P_i between the cell surface P_i pool and the intracellular P_i pool is affected by many factors, such as growth

stage, cellular P_i demand, and external P_i concentration (Fu et al., 2005). It can be seen from Figs. 2a and 3 that the ratio of intracellular P_i to the total P_i is low in the early stage of the experiment while higher in the exponential growth and maintenance phase of the cells, which is consistent with the previous research results (Jin et al., 2021; Sañudo-Wilhelmy et al., 2004; Saxton et al., 2012). Thus, during the high-incidence season of algal blooms, once QP/(QP+AP) of certain bloom-forming algae species exceeds a certain threshold, we can send out algal bloom warnings and take corresponding steps. Besides related to cell growth, the plasticity of QP/(QP+AP) also reflects the change in external P_i concentration at which the cells are grown. The total amount of surface-adsorbed P_i varies since the number of cell surface-binding sites exposed to DIP changes over time as external P_i concentration changes (Fig. 2d; (Fu et al., 2005; Saxton et al., 2012)). On the other hand, algal cells can adjust the level of intracellular P_i while maintaining a relatively stable growth rate for persistence across a range of P_i concentrations that do not allow for the accumulation of significant biomass (Saxton et al., 2012), which leads to the oscillations of Q and S (Fig. 2). Thus, stoichiometry flexibility on total P_i partitioning plays an essential role in the growth of microalgae in environments where nutrients are highly variable, for example, large lakes and estuarine systems (Davies & Wang, 2021; Saxton et al., 2012; Wang et al., 2008; Yuan et al., 2020).

To provide more accurate descriptions of P_i assimilation mechanism and phytoplankton growth characteristics in a changing environment, the model proposed in this paper can be further improved by considering some environmental factors, for example, solar irradiance, water velocity, environmental toxins, and the direct or indirect interactions of algal species (Xu et al., 2021; Yang & Yuan, 2021). This model is unlikely to apply to all algae, and the corresponding equation describing the

P_i uptake process needs to be established according to specific species. In general, combined with field data in the ocean, a prediction model tailored to the specific phytoplankton species of the target system will help to effectively predict the outbreak of harmful algal blooms.

CRediT authorship contribution statement

Anglu Shen: Conducted the experimental work, Data curation, Writing-original draft, Writing-review and editing, Funding acquisition. **Shufei Gao:** Data curation, Writing-original draft, Writing-review and editing. **Jie Jiang:** Data curation, Writing-original draft. **Qingjing Hu:** Writing-review and editing, Funding acquisition. **Hao Wang:** Conceptualization, Methodology, Writing-review and editing, Funding acquisition. **Sanling Yuan:** Conceptualization, Methodology, Writing-review and editing, Funding acquisition, Supervision.

Declaration of Competing Interest

The authors declare that they have no known competing financial interests or personal relationships that could have appeared to influence the work reported in this paper.

Data availability statement

All data used in this study can be found in the manuscript and its supplementary materials.

Acknowledgements

This work was supported by the National Key Research and Development Program of China (grant number 2019YFD0901401); National Natural Science Foundation of China (grant numbers

11671260; 12071293; 41506194); the Natural Sciences and Engineering Research Council of Canada (grant numbers RGPIN-2020-03911, RGPAS-2020-00090).

References

Adhurya, S., Das, S., Ray, S., & Fath, B. D. (2021). Simulating the effects of aquatic avifauna on the phosphorus dynamics of aquatic systems. *Ecol. Model.*, *445*, 109495. doi:10.1016/j.ecolmodel.2021.109495.

Anderson, D. M. (1997). Turning back the harmful red tide. *Nature*, *388*, 513–514. doi:10.1038/41415.

Anderson, D. M., Cembella, A. D., & Hallegraeff, G. M. (2012). Progress in understanding harmful algal blooms: paradigm shifts and new technologies for research, monitoring, and management. *Annu. Rev. Mar. Sci.*, *4*, 143–176. doi:10.1146/annurev-marine-120308-081121.

Anderson, D. M., Glibert, P. M., & Burkholder, J. M. (2002). Harmful algal blooms and eutrophication: nutrient sources, composition, and consequences. *Estuar.*, *25*, 704–726. doi:10.1007/BF02804901.

Bortz, D. M., & Nelson, P. W. (2004). Sensitivity analysis of a nonlinear lumped parameter model of hiv infection dynamics. *Bull. Math. Biol.*, *66*, 1009–1026. doi:10.1016/j.bulm.2003.10.011.

Button, D. K. (1978). On the theory of control of microbial growth kinetics by limiting nutrient concentrations. *Deep Sea Res.*, *25*, 1163–1177. doi:10.1016/0146-6291(78)90011-5.

Caperon, J. (1969). Time lag in population growth response of Isochrysis galbana to a variable nitrate environment. *Ecology*, *50*, 188–192. doi:10.2307/1934845.

Cembella, A. D., Antia, N. J., & Harrison, P. J. (1984). The utilization of inorganic and organic phosphorus compounds as nutrients by eukaryotic microalgae: A multidisciplinary perspective: Part 1. *Crc Crit. Rev. Microbiol.*, *11*, 13–81. doi:10.3109/10408418209113567.

Chen, N. S., & Chen, Y. (2021). Advances in the study of biodiversity of phytoplankton and red tide species in china (ii):the east china sea. *Oceanol. Limnol. Sinica*, *52*, 363–418 (in Chinese with English abstract).

Chen, T. Y., Yan, T., Wang, L. P., Zhang, B., & Zhou., M. J. (2007). The effect of the causative algae of large-scale HAB in the East China Sea on egg hatching of argopecten irradians, and population growth of *Brachionus plicatilis* and *Moina mongolica*. *Acta Oceanol. Sin.*, *26*, 112–122.

Cunningham, A., & Maas, P. (1978). Time lag and nutrient storage effects in the transient growth response of *Chlamydomonas reinhardii* in nitrogen-limited batch and continuous culture. *Microbiology*, *104*, 227–231. doi:10.1099/00221287-104-2-227.

Davies, C. M., & Wang, H. (2021). Contrasting stoichiometric dynamics in terrestrial and aquatic grazer–producer systems. *J. Biol. Dyn.*, *15*, S3–S34. doi:10.1080/17513758.2020.1771442.

Droop, M. R. (1973). Some thoughts on nutrient limitation in algae. *J. phycol.*, *9*, 264–272. doi:10.1111/j.1529-8817.1973.tb04092.x.

Droop, M. R. (1983). 25 years of algal growth kinetics a personal view. *Bot. Mar.*, *26*, 99–112. doi:10.1515/botm.1983.26.3.99.

Flynn, K. J. (2003). Modelling multi-nutrient interactions in phytoplankton; balancing simplicity and realism. *Prog. Oceanogr.*, *56*, 249–279. doi:10.1016/S0079-6611(03)00006-5.

Fu, F. X., Zhang, Y. H., Feng, Y. Y., & Hutchins, D. A. (2006). Phosphate and ATP uptake and growth kinetics in axenic cultures of the cyanobacterium *Synechococcus* CCMP 1334. *Eur. J. Phycol.*, *41*, 15–28. doi:10.1080/09670260500505037.

Fu, F. X., Zhang, Y. H., Leblanc, K., Sañudo-Wilhelmy, S. A., & Hutchins, D. A. (2005). The biological and biogeochemical consequences of phosphate scavenging onto phytoplankton cell surfaces. *Limnol. Oceanogr.*, *50*, 1459–1472. doi:10.4319/lo.2005.50.5.1459.

Gao, S. F., Shen, A. L., Jiang, J., Wang, H., & Yuan, S. L. (2022). Kinetics of phosphate uptake in the dinoflagellate *Karenia mikimotoi* in response to phosphate stress and temperature. *Ecol. Model.*, *468*, 109909. doi:10.1016/j.ecolmodel.2022.109909.

Gómez, F., Zhang, H., Rosellt, L., & Lin, S. J. (2021). Detection of *Prorocentrum shikokuense* in the mediterranean sea and evidence that *P. dentatum*, *P. obtusidens* and *P. shikokuense* are three different species (prorocentrales, dinophyceae). *Acta Protozool.*, *60*, 47–59. doi:10.4467/16890027AP.21.006.15380.

Guillard, R. R. L. (1975). Culture of phytoplankton for feeding marine invertebrates. In *Culture of marine invertebrate animals* (pp. 29–60). Springer. doi:10.1007/978-1-4615-8714-9_3.

Hallegraeff, G. M. (1993). A review of harmful algal blooms and their apparent global increase. *Phycologia*, *32*, 79–99. doi:10.2216/i0031-8884-32-2-79.1.

Jiang, J., Shen, A. L., Wang, H., & Yuan, S. L. (2019). Regulation of phosphate uptake kinetics in the bloom-forming dinoflagellates *Prorocentrum donghaiense* with emphasis on two-stage dynamic process. *J. Theor. Biol.*, *463*, 12–21. doi:10.1016/j.jtbi.2018.12.011.

Jin, J., Liu, S. M., & Ren, J. L. (2021). Phosphorus utilization by phytoplankton in the yellow sea during spring bloom: Cell surface adsorption and intracellular accumulation. *Mar. Chem.*, *231*, 103935. doi:10.1016/j.marchem.2021.103935.

John, E. H., & Flynn, K. J. (2000). Modelling phosphate transport and assimilation in microalgae; how much complexity is warranted? *Ecol. Model.*, *125*, 145–157. doi:10.1016/S0304-3800(99)00178-7.

Kay, R. W., & Mahlburg-Kay, S. (1991). Creation and destruction of lower continental crust. *Geol. Rundsch.*, *80*, 259–278. doi:10.1007/BF01829365.

Kilham, P., & Hecky, R. E. (1988). Comparative ecology of marine and freshwater phytoplankton. *Limnol. Oceanogr.*, *33*, 776–795. doi:10.4319/lo.1988.33.4part2.0776.

Kornberg, A., Rao, N. N., & Ault-Riche, D. (1999). Inorganic polyphosphate: a molecule of many functions. *Annu. Rev. Biochem.*, *68*, 89–125. doi:10.1146/annurev.biochem.68.1.89.

Lin, J. N., Song, J. J., Yan, T., Zhang, Q. C., & Zhou, M. J. (2015). Large-scale dinoflagellate bloom species *Prorocentrum donghaiense* and *Karenia mikimotoi* reduce the survival and reproduction of copepod *Calanus sinicus*. *J. Mar. Biol. Assoc. UK.*, *95*, 1071–1079. doi:10.1017/S0025315415000533.

Lin, J. N., Yan, T., Zhang, Q., Wang, Y. F., Liu, Q., & Zhou, M. J. (2014). In *situ* detrimental impacts of *Prorocentrum donghaiense* blooms on zooplankton in the East China Sea. *Mar. Pollut. Bull.*, *88*, 302–310. doi:10.1016/j.marpolbul.2014.08.026.

Lu, D. D., & Goebel, J. (2001). Five red tide species in genus Prorocentrum including the description

of *Prorocentrum donghaiense* lu sp. nov. from the east china sea. *Chin. J. Oceanol. Limn.*, *19*, 337–344 (in Chinese with English abstract). doi:10.1007/BF02850738.

Lu, S. H., & Li, Y. (2006). Nutritional storage ability of four harmful algae from the East China Sea. *Chinese Journal of Process Engineering*, *6*, 439 (in Chinese with English abstract).

Lu, S. H., Ou, L. J., Dai, X. F., Cui, L., Dong, Y. L., Wang, P. B., Li, D. M., & Lu, D. D. (2022). An overview of *Prorocentrum donghaiense* blooms in China: Species identification, occurrences, ecological consequences, and factors regulating prevalence. *Harmful Algae*, *114*, 102207. doi:10.1016/j.hal.2022.102207.

Marois, D. E., & Mitsch, W. J. (2016). Modeling phosphorus retention at low concentrations in florida everglades mesocosms. *Ecol. Model.*, *319*, 42–62. doi:10.1016/j.ecolmodel.2015.09.024.

Misra, A. K., Singh, R. K., Tiwari, P. K., Khajanchi, S., & Kang, Y. (2020). Dynamics of algae blooming: effects of budget allocation and time delay. *Nonlinear Dynam.*, *100*, 1779–1807. doi:10.1007/s11071-020-05551-4.

Muhammadu, B., Ranganathan, P., & Brennan, F. (2017). Dynamic modelling of microalgae cultivation process in high rate algal wastewater pond. *Algal Res.*, *24*, 457–466. doi:10.1016/j.algal.2016.10.016.

Ou, L. J., Wang, D., Huang, B. Q., Hong, H. S., Qi, Y. Z., & Lu, S. H. (2008). Comparative study of phosphorus strategies of three typical harmful algae in Chinese coastal waters. *J. Plankton Res.*, *30*, 1007–1017.

Parslow, J. S., Harrison, P. J., & Thompson, P. A. (1985). Interpreting rapid changes in uptake kinetics in the marine diatom *Thalassiosira pseudonana* (Hustedt). *J. Exp. Mar. Biol. Ecol.*, *91*, 53–64. doi:10.1016/0022-0981(85)90220-5.

Qu, Y., Jin, J., Xu, W., & Liu, S. (2020). Phosphorus assimilation process by dominant algae species in chinese coastal sea. *China Environ. Sci.*, *40*, 1257–1265 (in Chinese with English abstract).

Robarts, R. D., & Zohary, T. (1987). Temperature effects on photosynthetic capacity, respiration, and growth rates of bloom-forming cyanobacteria. *New Zeal. J. Mar. Fresh.*, *21*, 391–399. doi:10.1080/00288330.1987.9516235.

Sañudo-Wilhelmy, S. A., Tovar-Sanchez, A., Fu, F. X., Capone, D. G., Carpenter, E. J., & Hutchins, D. A. (2004). The impact of surface-adsorbed phosphorus on phytoplankton Redfield stoichiometry. *Nature*, *432*, 897–901. doi:10.1038/nature03125.

Saxton, M. A., Arnold, R. J., Bourbonniere, R. A., Mckay, R. M., & Wilhelm, S. W. (2012). Plasticity of Total and Intracellular Phosphorus Quotas in *Microcystis aeruginosa* Cultures and Lake Erie Algal Assemblages. *Front. Microbiol.*, *3*, 3. doi:10.3389/fmicb.2012.00003.

Schindler, D. W., Hecky, R. E., Findlay, D. L., Stainton, M. P., Parker, B. R., Paterson, M. J., Beaty, K. G., Lyng, M., & Kasian, S. E. M. (2008). Eutrophication of lakes cannot be controlled by reducing nitrogen input: results of a 37-year whole-ecosystem experiment. *P. Natl. Acad. Sci.*, *105*, 11254–11258. doi:10.1073/pnas.0805108105.

Shen, A. L., Chen, W. W., Xu, Y. J., & Ho, K. C. (2022). Zooplankton population and community structure changes in response to a harmful algal bloom caused by *Prorocentrum donghaiense* in the East China Sea. *J. Mar. Sci. Eng.*, *10*, 291. doi:10.3390/jmse10020291.

Shen, A. L., Ishizaka, J. J., Yang, M. M., Ouyang, L. L., Yin, Y., & Ma, Z. L. (2019). Changes in community structure and photosynthetic activities of total phytoplankton species during the growth, maintenance, and dissipation phases of a *Prorocentrum donghaiense* bloom. *Harmful Algae*, *82*, 35–43. doi:10.1016/j.hal.2018.12.007.

Shen, A. L., Ma, Z. L., Jiang, K. J., & Li, D. J. (2016). Effects of temperature on growth, photophysiology, rubisco gene expression in *Prorocentrum donghaiense* and *Karenia mikimotoi*. *Ocean Sci. J.*, *51*, 581–589. doi:10.1007/s12601-016-0056-2.

Shi, P. L., Shen, H., Wang, W. J., Chen, W. J., & Xie, P. (2015). The relationship between light intensity and nutrient uptake kinetics in six freshwater diatoms. *J. Environ. Sci.*, *34*, 28–36. doi:10.1016/j.jes.2015.03.003.

Solovchenko, A. E., Ismagulova, T. T., Lukyanov, A. A., Vasilieva, S. G., & Gorelova, O. A. (2019). Luxury phosphorus uptake in microalgae. *J. Appl. Phycol.*, *31*. doi:10.1007/s10811-019-01831-8.

Sun, K., Qiu, Z. F., He, Y. J., & Yin, B. S. (2014). Nutrient-controlled growth of *Skeletonema costatum*: an applied model. *Chin. J. Oceanol. Limn.*, *32*, 608–625 (in Chinese with English abstract). doi:10.1007/s00343-014-3201-8.

Tang, D. L., Di, B. P., Wei, G. f., Ni, I.-H., Oh, I. S., & Wang, S. F. (2006). Spatial, seasonal and species variations of harmful algal blooms in the South Yellow Sea and East China Sea. *Hydrobiologia*, *568*, 245–253. doi:10.1007/s10750-006-0108-1.

Tester, P. A., & Steidinger, K. A. (1997). *Gymnodinium breve* red tide blooms: initiation, transport,

and consequences of surface circulation. *Limnol. Oceanogr.*, *42*, 1039–1051. doi:10.4319/lo.1997.42.5_part_2.1039.

Tiwari, P. K., Misra, A. K., & Venturino, E. (2017). The role of algae in agriculture: a mathematical study. *J. Biol. Phys.*, *43*, 297–314. doi:10.1007/s10867-017-9453-8.

Uye, S., Iwamoto, N., Ueda, T., Tamaki, H., & Nakahira, K. (1999). Geographical variations in the trophic structure of the plankton community along a eutrophic–mesotrophic–oligotrophic transect. *Fish. Oceanogr.*, *8*, 227–237. doi:10.1046/j.1365-2419.1999.00110.x.

Wang, H., Garcia, P. V., Ahmed, S., & Heggerud, C. M. (2022). Mathematical comparison and empirical review of the monod and droop forms for resource-based population dynamics. *Ecol. Model.*, *466*, 109887. doi:10.1016/j.ecolmodel.2022.109887.

Wang, H., Kuang, Y., & Loladze, I. (2008). Dynamics of a mechanistically derived stoichiometric producer-grazer model. *J. Biol. Dyn.*, *2*, 286–296. doi:10.1080/17513750701769881.

Wang, H., Smith, H. L., Kuang, Y., & Elser, J. J. (2007). Dynamics of stoichiometric bacteria-algae interactions in the epilimnion. *SIAM J Appl. Math.*, *68*, 503–522. doi:10.1137/060665919.

Xiao, X., Agusti, S., Pan, Y. R., Yan, Y., Li, K., Wu, J. P., & Duarte, C. M. (2019). Warming amplifies the frequency of harmful algal blooms with eutrophication in chinese coastal waters. *Environ. Sci. Technol.*, *2019*, 13031–13041. doi:10.1021/acs.est.9b03726.

Xing, Y. F., Guo, L., Wang, Y., Zhao, Y. G., Jin, C. J., Gao, M. C., Ji, J. Y., & She, Z. L. (2021). An insight into the phosphorus distribution in extracellular and intracellular cell of *chlorella vulgaris* under mixotrophic cultivation. *Algal Res.*, *60*, 102482. doi:10.1016/j.algal.2021.102482.

494 Xu, C. Q., Yuan, S. L., & Zhang, T. H. (2021). Competitive exclusion in a general multi-
495 species chemostat model with stochastic perturbations. *Bull. Math. Biol.*, *83*, 1–17. doi:10.
496 1007/s11538-020-00843-7.

497 Xu, W. Q., & Liu, S. M. (2016). Phytoplankton responses to phosphorus in Sanggou Bay in spring
498 and autumn. *Adv. Mar. Sci.*, *3*, 26–37. doi:10.12677/ams.2016.32005.

499 Yang, J. G., & Yuan, S. L. (2021). Dynamics of a toxic producing phytoplankton-zooplankton
500 model with three-dimensional patch. *Appl. Math. Lett.*, *118*. doi:10.1016/j.aml.2021.107146.

501 Yao, B., Xi, B. D., Hu, C. M., Huo, S. L., Shu, J., & Liu, H. L. (2011). A model and experimental
502 study of phosphate uptake kinetics in algae: considering surface adsorption and P-stress. *J.*
503 *Environ. Sci.*, *23*, 189–198. doi:10.1016/S1001-0742(10)60392-0.

504 Yu, R. C., Zhang, Q. C., Kong, F. Z., Zhou, Z. X., Chen, Z. F., Zhao, Y., Geng, H. X., Dai, L.,
505 Yan, T., & Zhou, M. J. (2017). Status, impacts and long-term changes of harmful algal blooms in
506 the sea area adjacent to the Changjiang River estuary. *Oceanol. Limnol. Sinica*, *48*, 1178–1186
507 (in Chinese with English abstract).

508 Yuan, S. L., Wu, D. M., Lan, G. J., & Wang, H. (2020). Noise-induced transitions in a nonsmooth
509 producer–grazer model with stoichiometric constraints. *Bull. Math. Biol.*, *82*, 1–22. doi:10.1007/
510 s11538-020-00733-y.

511 Zhao, D. Z. (2010). Occurrence regularity of marine red tide disaster in typical areas in China.
512 Marine Press, Beijing.

513 Zhou, Y., Nguyen, B. T., Zhou, C., Straka, L., Lai, Y. J. S., Xia, S. Q., & Rittmann, B. E. (2017a).

514 The distribution of phosphorus and its transformations during batch growth of *synechocystis*.
515 *Water Res.*, *122*, 355–362. doi:10.1016/j.watres.2017.06.017.

516 Zhou, Z. X., Yu, R. C., & Zhou, M. J. (2017b). Resolving the complex relationship between harmful
517 algal blooms and environmental factors in the coastal waters adjacent to the Changjiang River
518 estuary. *Harmful Algae*, *62*, 60–72. doi:10.1016/j.hal.2016.12.006.

519 Zhou, Z. X., Yu, R. C., & Zhou, M. J. (2017c). Seasonal succession of microalgal blooms from
520 diatoms to dinoflagellates in the East China Sea: A numerical simulation study. *Ecol. Model.*,
521 *360*, 150–162. doi:10.1016/j.ecolmodel.2017.06.027.